Hindawi
Advances in Materials Science and Engineering
Volume 2023, Article ID 9089620, 14 pages
https://doi.org/10.1155/2023/9089620

Research Article

Stir Casting Processing, Mechanical, and Wear Behavior of AA2024 +10 wt. % Flyash +5 wt. % Graphite Hybrid Composite

S. Senthil Murugan,[1] **M. Vigneshkumar**,[2] **M. John Iruthaya Raj**,[3] **Sivamani Selvaraju**,[4] **N. Vinayaka**,[5] **Srinivasan Murugan**,[6] **V. Vijayan**,[7] **and Addisalem Mekonnen**[8]

[1]*Department of Mechanical Engineering, Rajalakshmi Engineering College, Chennai 602105, Tamilnadu, India*
[2]*Department of Mechanical Engineering, Sri Krishna College of Engineering and Technology, Coimbatore, Tamilnadu, India*
[3]*Department of Mechanical Engineering, Mar Ephraem College of Engineering and Technology, Marthandam, Tamilnadu, India*
[4]*Department of Engineering, University of Technology and Applied Sciences, Salalah, Oman*
[5]*Department of Aeronautical Engineering, Nitte Meenakshi Institute of Technology, Yelahanka, Bengaluru 560064, India*
[6]*Department of Mechanical Engineering, Mahendra Engineering College, Mahendrapuri, Mallasamudram, Namakkal 637503, India*
[7]*Department of Mechanical Engineering, K. Ramakrishnan College of Technology, Samayapuram, Trichy, Tamil Nadu, India*
[8]*Department of Mechanical Engineering, Faculty of Manufacturing Institute of Technology, Hawassa University, Hawassa, Ethiopia*

Correspondence should be addressed to Addisalem Mekonnen; addisalemm@hu.edu.et

Received 12 August 2022; Revised 10 October 2022; Accepted 25 November 2022; Published 9 February 2023

Academic Editor: Pudhupalayam Muthukutti Gopal

Metal matrix composites (MMCs) and their hybrid combinations are widely incorporated in research due to their enhanced mechanical properties and wear resistance. In this work, an investigation is made to fabricate AA2024 matrix flyash and graphite-reinforced hybrid composite for industrial applications and determine its suitability by performing testing and characterization. Tensile properties and compressive strength, wear resistance, fracture toughness, impact energy, and the hardness of the composites are evaluated. A tensile strength maximum of 300 MPa was achieved. Furthermore, the thermal analysis of a disc brake of this hybrid composite is performed using SOLIDWORKS software to identify the temperature distribution up to 469°K. The addition of flyash reinforcement shows the changes in properties with weight reduction. Although the content of graphite particles shows a deterioration in mechanical properties, it acts as a lubricant and reduces wear by friction and friction between the components. The coefficient of friction (COF) for the specimen is in the range of 0.1 to 0.3. The distribution of graphite and flyash is analyzed using the scanning electron microscope. It was found that the properties of the prepared composite are lesser than the base alloy AA2024, but the fabricated composite's density (2.07 g/cc) is lesser than the base alloy AA2024 (2.78 g/cc).

1. Introduction

The possibilities of obtaining a desirable blend of strength, rigidity, toughness, or specific weight using traditional materials are limited. Composite materials have gained significant attraction in recent times for overcoming these inadequacies and meeting the excessive requirements of today's technology. MMCs have considerably enhanced properties over conventional alloys, such as high specific strength, specific modulus, dampening capacity, and abrasion resistance [1]. Some of MMCs' physical properties, such as their lack of significant moisture absorption, reduced thermal conductivities, and resistance to most radiations, are also advantageous. Composites with low-density and low-cost reinforcing are becoming increasingly popular [2, 3]. Composites reinforced with flyash are anticipated to break through the cost barrier for broad use in automobile and light-duty applications [4]. As a result, it is anticipated that

integrating flyash particles into aluminium alloys leads to an effective application for the low-cost waste by-product and also the capacity to preserve energy-intensive consuming aluminium components [5]. Particulate reinforced aluminum matrix composites are gaining popularity due to their low cost and benefits such as isotropic characteristics and the ability to undergo secondary processing, allowing for the creation of secondary components [6]. Cast aluminum matrix particle reinforced composites offer higher specific strength, specific modulus, and wear resistance than unreinforced alloys [7]. The shortcoming of aluminium alloys is the minimal resistance to abrasive wear under low-lubrication conditions and their significant retention of the lubricating layer over the sliding surface, making tribological applications difficult. Aluminium graphite particle composites are self-lubricating composites that receive attention from researchers because of their remarkable anti-seizure effect, high thermal stability, excellent damping characteristics, and reduced friction coefficient [8]. This self-lubrication is caused by the shearing of graphite particles under the composite's sliding surface, which reduces shear stress, alleviates permanent deformation in the subsurface area, reduces the friction coefficient, and acts as a lubricant [9]. As a result, the development and retention of this tribo-layer on the sliding surface influence the materials' tribological behavior through material properties such as chemical composition, mode of fracture, and material thickness [10]. It is determined by the type of sliding surface, the atmosphere, and the amount of graphite content in the composite. It has been observed that increasing the graphite component in Al/graphite composites reduces the wear rate. However, there are claims that the wear rate increases with the graphite content owing to a reduction in the fracture toughness and hardness of composites [11]. Hence, extensive experimental research is required to analyze the effect of the inclusion of micron-size flyash and graphite with the matrix AA2024 wrought alloy.

The novelty of the paper is the hybrid combination of flyash with graphite reinforcement, and the aim of the present work is to fabricate the AA2024 aluminum matrix hybrid composite using the stir casting setup and to characterize the fabricated specimens, including the thermal analysis using SOLIDWORKS software.

2. Materials and Method

Aluminum AA2024 alloy is the matrix for the hybrid aluminum matrix composite in the current study. It is utilized in applications, which demand a high strength-to-weight ratio, in addition, to excellent fatigue resistance such as wings and fuselages in aircraft structures. The chemical composition of the alloy as per optical emission spectroscopy is presented in Table 1. Flyash is one of the wastes produced by coal burning. The principal elements of flyash are oxides such as SiO_2, Al_2O_3, and Fe_2O_3, which are present in the industrial by-product collected from the flue gas of coal-burning electric power plants. It is widely used by the construction industry for cost reduction in the manufacturing of concrete structures, bricks as well as road construction. The composition of different fly ashes is presented in Table 2. Graphite nature is soft and it has a lubrication property [11].

The stir casting method was utilized for the preparation of AA2024 metal matrix composite as both class-F flyash (100 grams = 10%), and graphite (50 grams = 5%) were the reinforcements. Figure 1(a) shows the stir-casting process. The fabrication of a composite involves the addition of dispersed phases into a molten matrix and subsequent solidification. Initially, the mold for the casting and the reinforcement particles at the required weight was preheated to 200°C in an oven. The aluminum AA2024 (1000 grams) was melted in the clay crucible in the furnace and followed by the addition of reinforcement into the molten matrix, which is at 680°C–700°C slowly with a rate of 1 gram per 20 sec. The temperature was ensured with a thermocouple and digital meter. During the stirring with a stirrer, the chemical reaction took place between the matrix alloy and reinforcement to develop homogeneous hybrid composites. The stir casting setup is utilized to achieve excellent mechanical properties owing to the increased interfacial bonding among the matrix and flyash through the vortex developed. Once the proper mixture is obtained, then the temperature is measured and the prepared composite was poured at the temperature of 780°C into the preheated mold (Figure 1(b)). Three molds are prepared for casting rods of a diameter of 20 mm, length of 300 mm, and length of 350 mm, as shown in Figure 1(c). The required specimens were cut from the cast for the characterization of microstructures, tensile, compression, and hardness testing. Wear rate analysis was also performed on the prepared specimens. The cast rods are first cut into various lengths according to the specifications. Now, the cut pieces are machined in the lathe. The specimen for the tensile test involves turning, facing, and chamfering. The specimens for the compression test and wear tests involve turning and facing. It is found that the density of the hybrid composite is lesser than that of the base alloy AA2024. Thus, the weight is automatically reduced. Theoretical and experimental density values of the hybrid composite fabricated are 1.97 g/cm^3, and 2.077 g/cm^3, respectively. These values are lesser than the density of AA2024 value of 2.78 g/cm^3.

3. Testing, Results, and Discussion

3.1. Tensile Test. In the tensile test, the specimens are subjected to uniaxial tension until failure. Figures 2(a)–2(d) show the tensile testing (ASTM E8 standard) of the prepared composite. The tensile sample for testing was prepared as per the standard given in Figure 2(a). The prepared tensile specimen and the specimen position in the testing machine are given in Figures 2(b) and 2(c), respectively. The tensile fractured specimens are shown in Figure 2(d). The neck formation was not seen on the specimens after tensile testing. The recorded stress and strain curve during tensile testing is given in Figure 3(a). The tensile testing result was almost the same for all three samples according to the stress vs strain curve. It showed the ultimate stress was around 300 MPa and the strain of around the 3.6–3.8 range. The

Table 1: Chemical composition of AA2024 matrix.

Element	Al	Cu	Fe	Mg	Mn	Si	Ti	Ni	Zn	Cr	Pb	Sn
%	91.95	4.63	0.35	1.4	0.6	0.41	0.05	0.01	0.2	0.38	0.04	0.03

Table 2: Composition of various fly ashes.

Component	Bituminous	Sub-bituminous	Lignite
SiO_2 (%)	20–60	40–60	15–45
Al_2O_3 (%)	5–35	20–30	20–25
Fe_2O_3 (%)	10–40	4–10	4–15
CaO (%)	1–12	5–30	15–40
LOI (%)	0–15	0–3	0–5

ultimate tensile and yield strength were observed and given in the bar chart shown in Figure 3(b). The values are noted for three specimens, and the average value is considered the final value. The average tensile and yield strengths were 297 MPa and 154 MPa, respectively. The composite strength is lesser than that of the AA2024 alloy. The reason is though the graphite and flyash reduce the weight of the composites, it decreases the composite strength. The strain hardening rate (h) was calculated based on the values of yield strength (YS), and tensile strength (TS) of the prepared casting. It decides the material ductility and is also an important property for engineering applications [12]. It can vary depending on the strain rate. The estimated YS/TS ratio and TS and YS difference are plotted in Figures 3(c) and 3(d), respectively. The decrease in this YS/TS ratio means an increase in tensile ductility. The value here is in the range of 0.5. Although all the samples have almost equal values, sample 1 shows the maximum ductility with a 0.513 ratio value. These values might be considered for the evaluation of the strain-hardening exponent of the composite. Similarly, the difference in tensile and yield strength has an impact on the plastic deformation of the castings. From the data, the values are in the range of 141 to 143 MPa. Here, sample 1 showed a maximum value of 143.8 MPa. According to Von Mises's statement, shear yield strength (τ) can be estimated by Von Mises's yield criterion (equation (1)) [13]. Maximum shear yield strength is 79 MPa for sample 2 and a minimum of 75.8 MPa.

$$\tau = 0.5\sigma_{ys}, \tag{1}$$

where "τ" is the shear yield stress in MPa, σ_{ys}-yield strength in MPa.

3.2. Compression Test. The compression test is conducted in the UTM (Universal Testing Machine). Here, the specimen is subjected to a uni-axial compression until failure. Compressive strength is the ability of a material to bear a compressive load tending to reduce its height. As per Figure 4(a), the compressive test specimen ($100\,\text{mm} \times \phi 20\,\text{mm}$) was prepared as per ASTM E9 standard and the specimen is shown in Figure 4(b). The Specimen after the compressive test is shown in Figure 4(c), and the crack was found in the center of the specimens. The compressive test results are given in Figure 5(a). Figures 5(b) and 5(c) show the load vs displacement curve and stress vs strain curve for all three specimens, respectively. The ultimate compressive load and ultimate compressive strength are taken from the graphs generated for the specimens. The values are noted, and the average of the three values is considered the final value. The average ultimate load was 72.5 kN, and the average ultimate compressive strength was 267.3 MPa. It is found that the compressive strength gets reduced with that of the base alloy AA2024. During compressive testing, the maximum load was obtained as 80 kN, and the maximum compressive strength was recorded as 300 MPa. From the graph, the load obtained was in the range between 48 and 80 kN, whereas the stress value during compressive testing was in the range of 180 MPa–30 MPa, as per plots Figures 5(b) and 5(c). The crack was found in the compressed samples. The convex portion propagates cracks and was highly affected by the compressive load during the compression test.

3.3. Toughness Test. The toughness of the composite is determined by the Charpy impact test to analyze the amount of energy absorbed by the prepared casting during fracture. This study helps to study the ductile to brittle transition on the material. Here, the impact test was done on the prepared casting specimen ($10\,\text{mm} \times 10\,\text{mm} \times 55\,\text{mm}$) shown in Figure 6(a). A V-notch was cut to a depth of 2 mm at the center. The Charpy impact test was taken for three specimens, and the impact energy was noted, as shown in Figure 6(b). The average value was around 1.52 kg·m. The toughness value gets reduced when compared to that of base alloy AA2024. The specimen subjected to impact is shown in Figure 6(c). The Rolfe Novak Barsom upper shelf correlation [14–16] is given in equation (2) [17]. Using this equation, the fracture toughness was calculated with impact energy. The recorded fracture toughness values are given as a bar chart in Figure 6(d). The values were in the range of 24.8 to 25.4 $\text{MPa}\cdot\text{m}^{1/2}$. The average fracture toughness was about 24.99 $\text{MPa}\cdot\text{m}^{1/2}$.

$$\left(\frac{K}{Y_s}\right)^2 = 5\left[\left(\frac{I}{Y_s}\right) - 0.05\right], \tag{2}$$

where "K" is fracture toughness ($\text{MPa}\cdot\text{m}^{1/2}$) [18], "$Y_S$" is yield strength (MPa), and "I" is impact energy (kg·m)

3.4. Hardness Test. A hardness test is performed to determine the ability of the composite material to withstand indentation [19]. The Rockwell hardness test (B scale) is used in our current study to determine the hardness, which is based on the depth of penetration of an indenter. The indentation on the specimen is shown in Figure 7(b). The hardness value is taken at three different spots. The average of the three values is taken as the final value and shown in

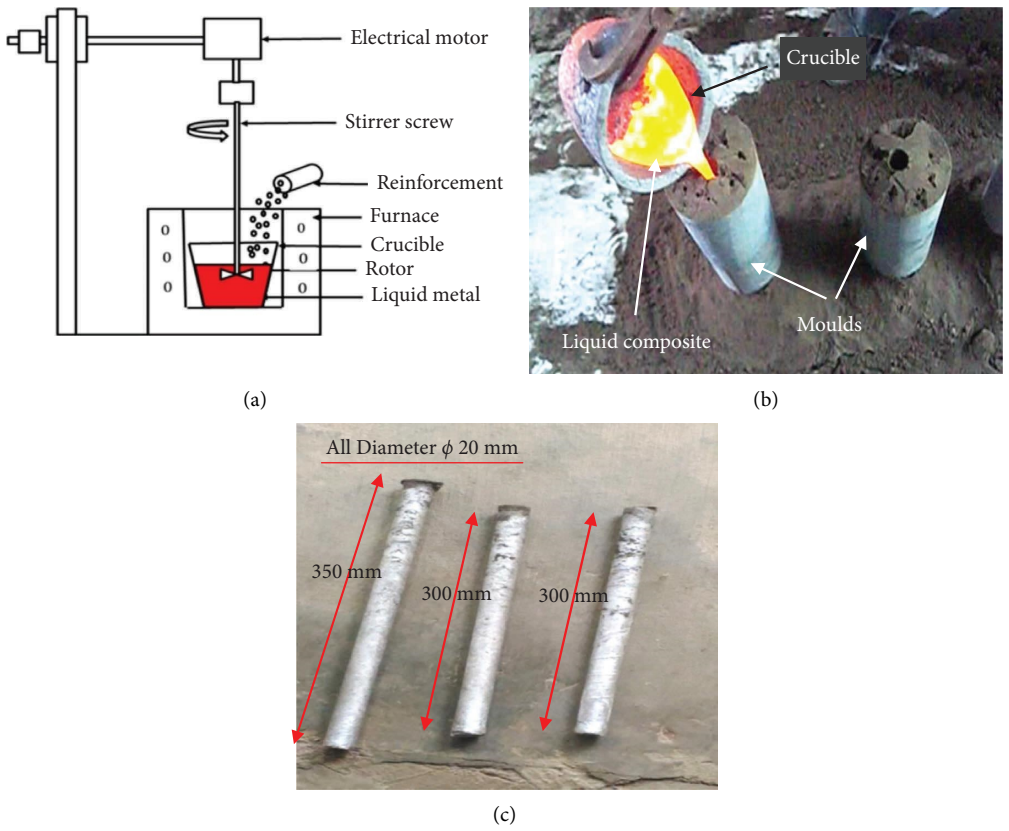

Figure 1: (a) Schematic of stir casting; (b) composite pouring; (c) prepared composite castings.

Figure 7(c) for samples 1, 2, and 3. It was found that the hardness of the hybrid composite was lesser than that of the base alloy AA2024. An average of 63HRB hardness was recorded.

3.5. Wear Test. The tribological experiments were conducted at a temperature of 30°C using the pin-on-disc apparatus seen in Figure 8(a). The tests were carried out at a 500 rpm sliding speed, a 20 N applied force, and a distance of 1000 m. For the wear test, pins having a diameter of 10 mm and a height of 30 mm were employed, as indicated in Figure 8(a). The specimen for wear testing is given in Figure 8(b). The surface of the pin was polished, as shown in Figure 8(c), and was rotated against a disc. The specimen after the wear testing is shown in Figure 8(d). The wear rate was determined by observing the loss of weight during the testing. A digital weighing scale with an accuracy of 0.1 mg was used to determine the weight of each specimen. Weight loss is defined as the difference in weight of the test specimen before and after testing. A graphite lubricating coating covers the whole worn surface, eliminating direct interaction between the pin and disc and lowering the friction coefficient significantly. The friction coefficient and wear rate for three distinct specimens were determined, and the final result was calculated using the average of the three data. It is found that wear properties have shown improvement due to the addition of graphite. The wear rate and friction coefficient values are presented in Table 3. The coefficient of friction (COF) was calculated using (3) [20], where the applied load/normal force (L_a) in "N" was 20 N and the frictional force (F_f) in "N."

$$\text{COF} = \frac{F_f}{L_a}. \tag{3}$$

By physically examining the test specimens before and after wear testing, the changes in the cross-sectional area of the specimens were easily comprehended. Very few weight losses (in grams) were observed among all three specimens. The composite (sample 1) showed higher COF. A higher COF means that more/higher F_f was present. Here, the COF was less than 0.5, and its range was 0.1 to 0.3. If the COF value is greater than 1, it means that the normal force is weaker than the friction. Here, the addition of graphite reduced the COF value. From the results, low COF showed a high wear rate.

Figure 9 provides the relationship of frictional force over sliding distance during the wear analysis of all three samples. For sample 1, the frictional force reached 6.5 N; whereas it reached for samples 2 and 3 to 5.7 N and 3.2 N, respectively. COF and wear rate are the functions of sliding distance [21]. The wear rate and the weight loss values are low for high frictional force. There are not many variations in the frictional forces in the due course of the period while increasing the sliding distance from 300 mm onwards. The value might be changing according to the changes in the applied load.

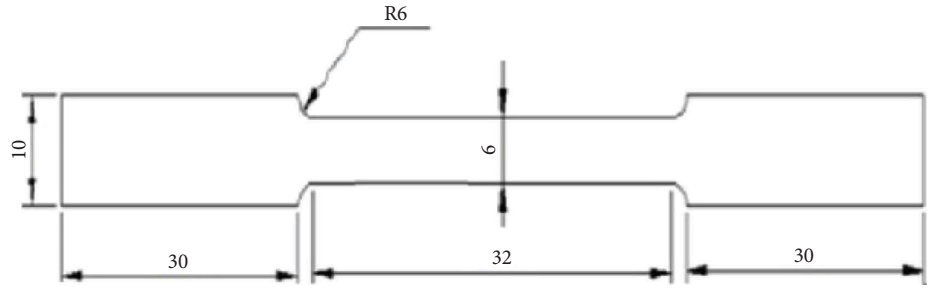

(a)

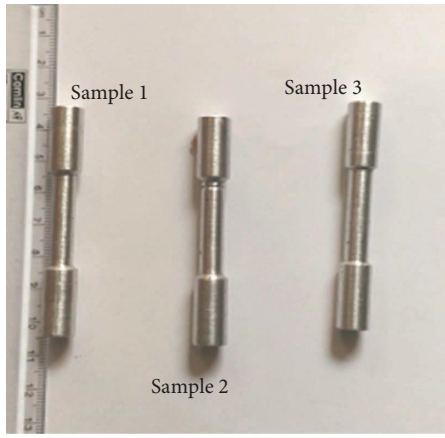

(b)

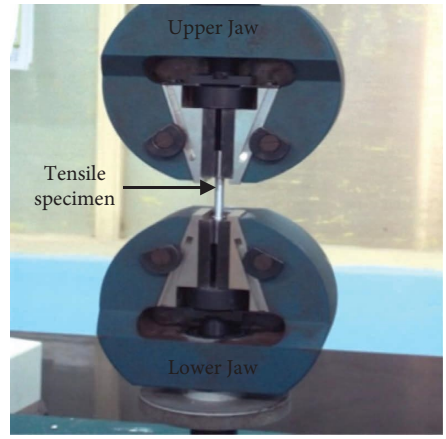

(c)

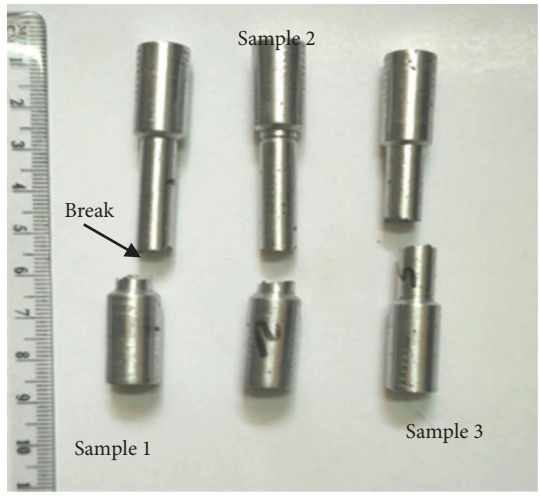

(d)

Figure 2: (a) Tensile sample dimension; (b) prepared cast samples for tensile testing; (c) tensile testing in the UTM machine; (d) specimen after tensile test.

3.6. Microstructure. The scanning electron microscope (SEM) that was used for this study is shown in Figure 10(a). By utilizing a concentrated electron beam across the surface of the material, the image is shown in Figure 10(b) was taken at 25 μm size on the surface of the finished specimen to analyze its surface properties and access the dispersion of flyash and graphite. From the microstructure analysis, the distribution of flyash on the surface of the composite is observed. It also shows the formation of pores and graphite accumulation on the surface. The accumulation of graphite on the surface forms a lubricating layer so that it reduces the wear rate by reducing the contact area and reducing the strength and hardness also.

3.7. Thermal Analysis. The prepared hybrid composite can be used in the application of disc brakes in automotive applications. Thermal analysis (Figures 11(a)–11(d)) was carried out for a disc brake using SOLIDWORKS software. Thermal analysis was done for finding out the temperature

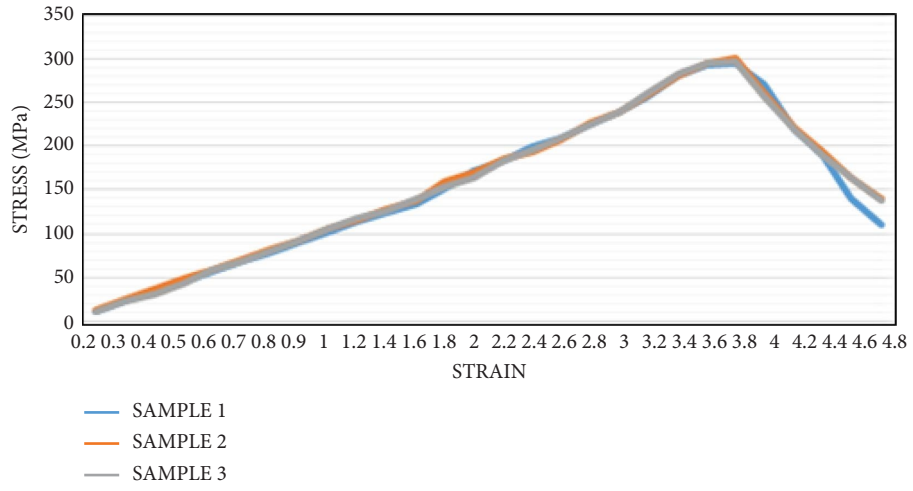

(a)

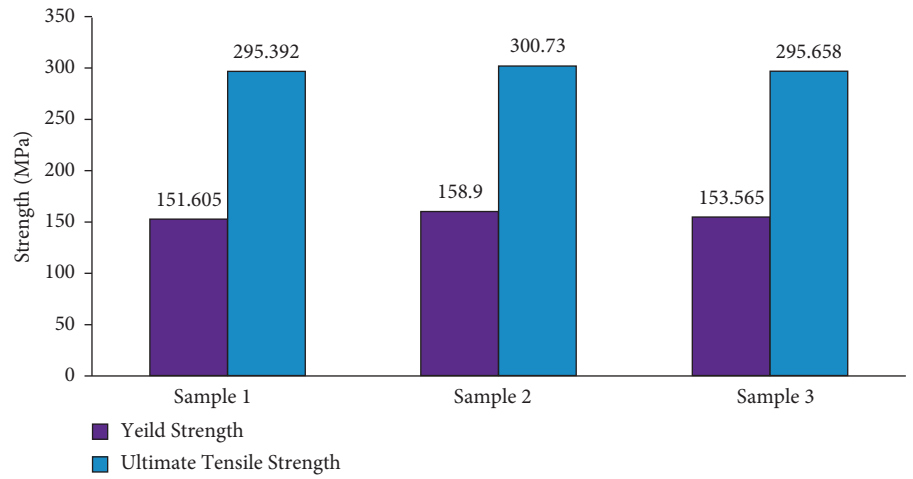

(b)

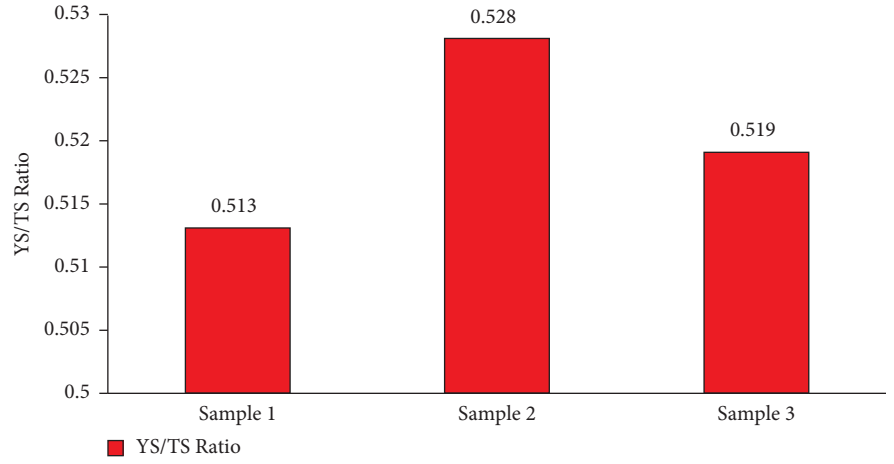

(c)

Figure 3: Continued.

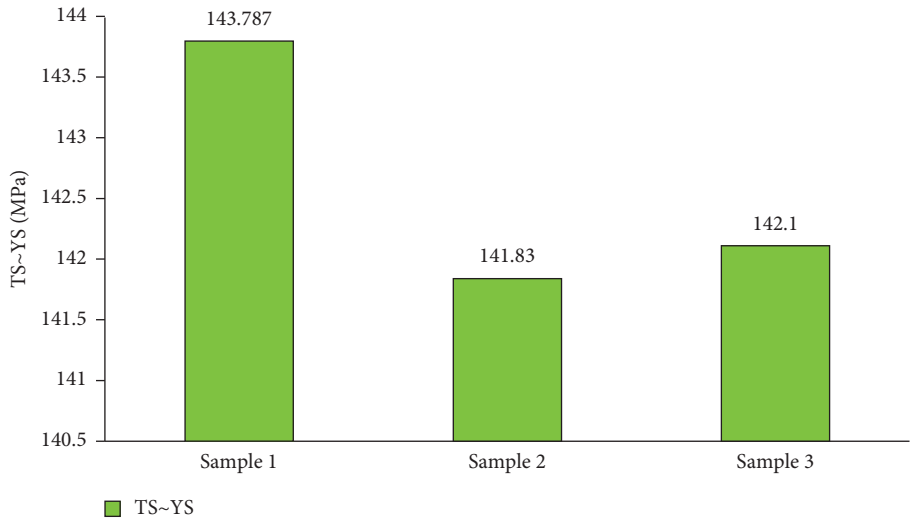

(d)

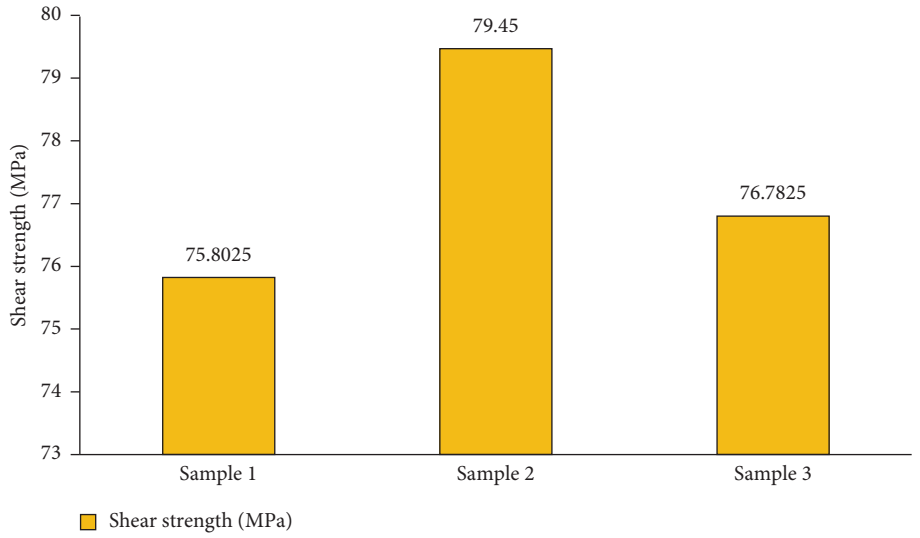

(e)

Figure 3: (a) Stress vs. strain curve for 3 specimens; (b) tensile and yield strength; (c) YS/TS ratio; (d) TS–YS variation; (e) estimated shear strength.

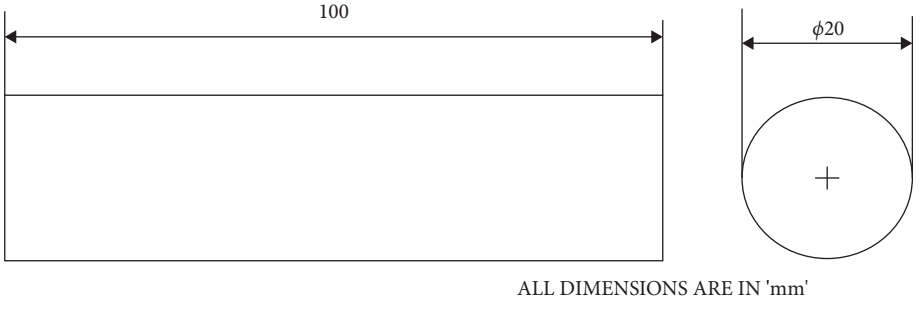

(a)

Figure 4: Continued.

(b)

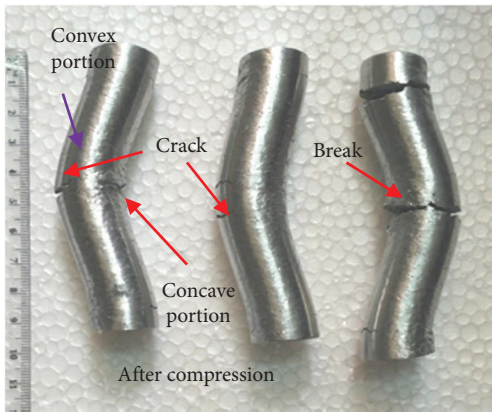

(c)

Figure 4: (a) Compression test specimen dimension; (b) specimen prepared for the compressive test; (c) samples after compression test.

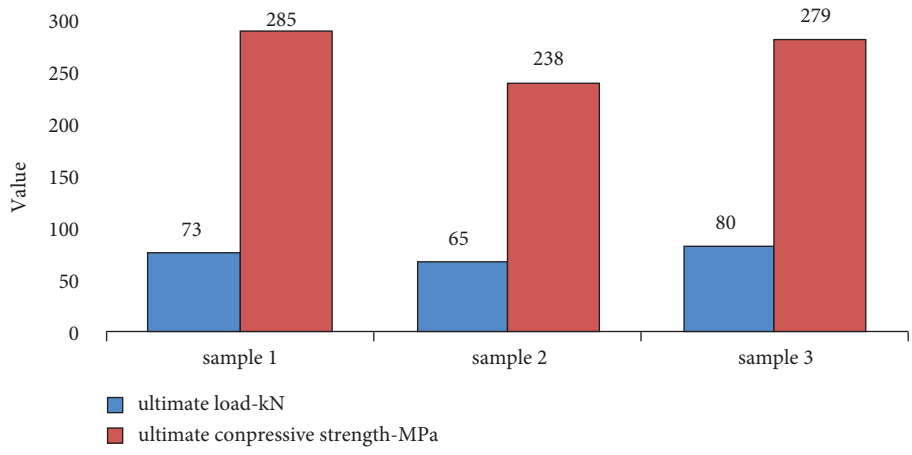

(a)

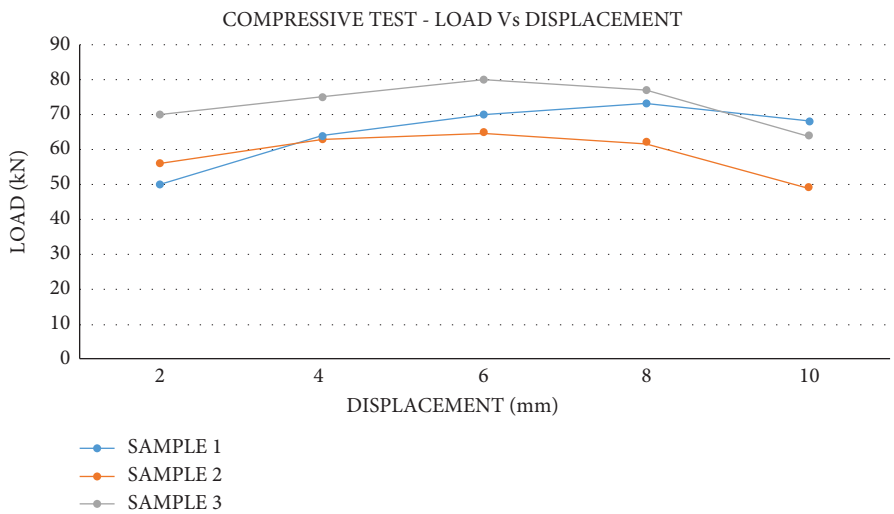

(b)

Figure 5: Continued.

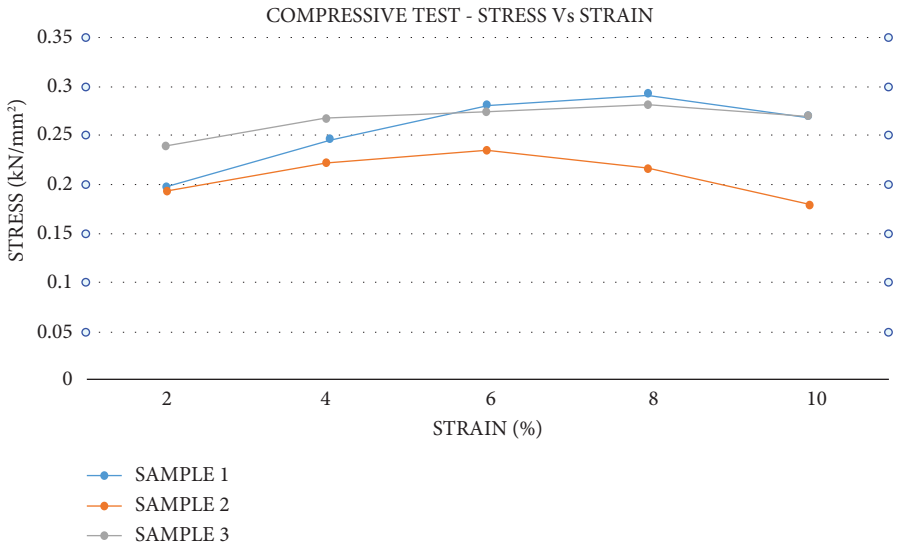

(c)

Figure 5: (a) Compressive test results; (b) relationship of load and displacement for the composites; (c) stress vs. strain curve for the compressive test.

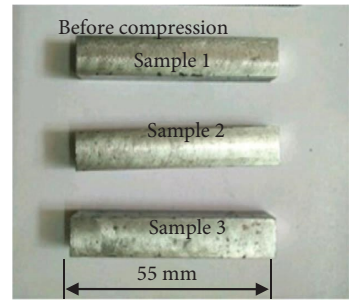

(a)

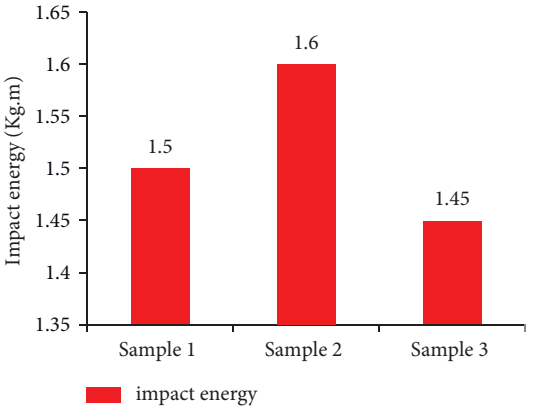

(b)

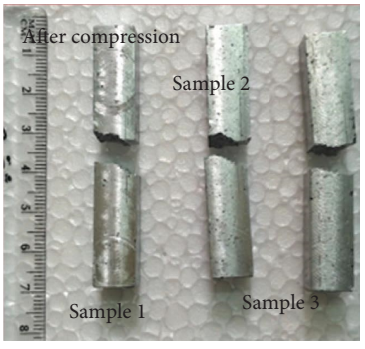

(c)

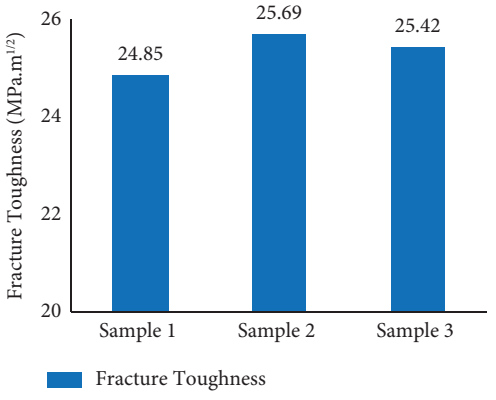

(d)

Figure 6: (a) Charpy test specimen before V-notching; (b) impact energy values of the composite specimen; (c) specimen after Charpy test; (d) fracture toughness of composite specimens.

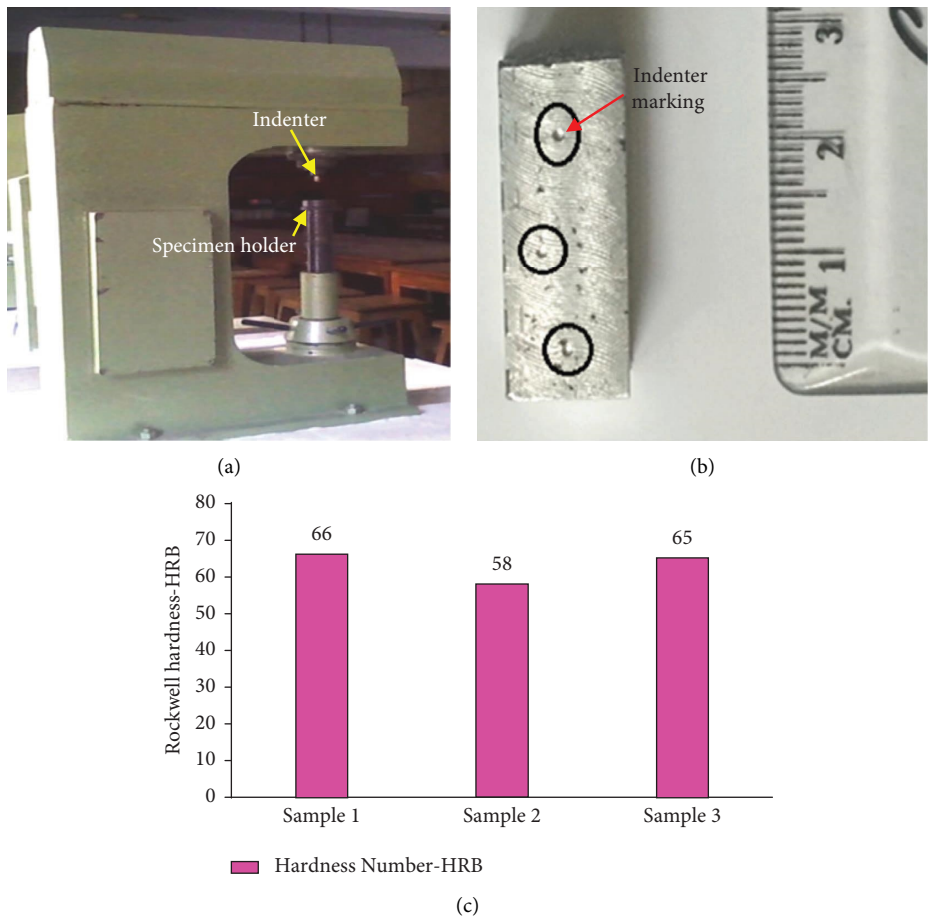

Figure 7: (a) Rockwell hardness tester; (b) hardness specimen; (c) hardness test results.

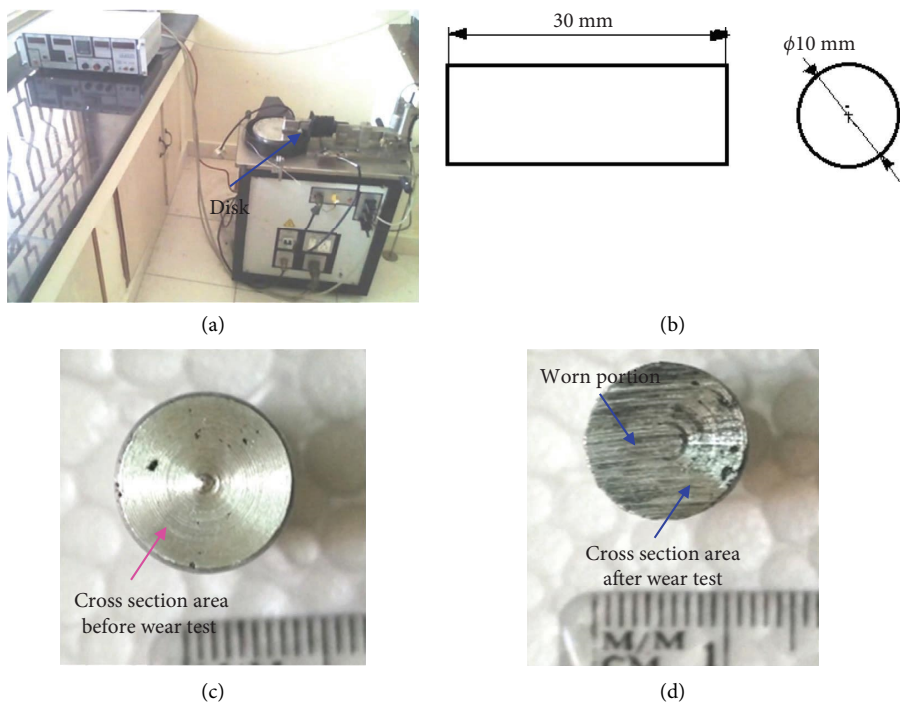

Figure 8: (a) Pin-on-disc apparatus; (b) wear test specimen design; (c) before wear test; (d) after wear test.

Table 3: Wear test readings.

Specimen	Initial weight (gm)	Final weight (gm)	Weight loss (gm)	Coefficient of friction	Wear rate (mm^3/Nm)
Sample 1	6.3250	6.3130	0.0120	0.325	0.00028888
Sample 2	6.4877	6.4754	0.0123	0.285	0.0002961
Sample3	6.3487	6.3360	0.0127	0.185	0.0003057

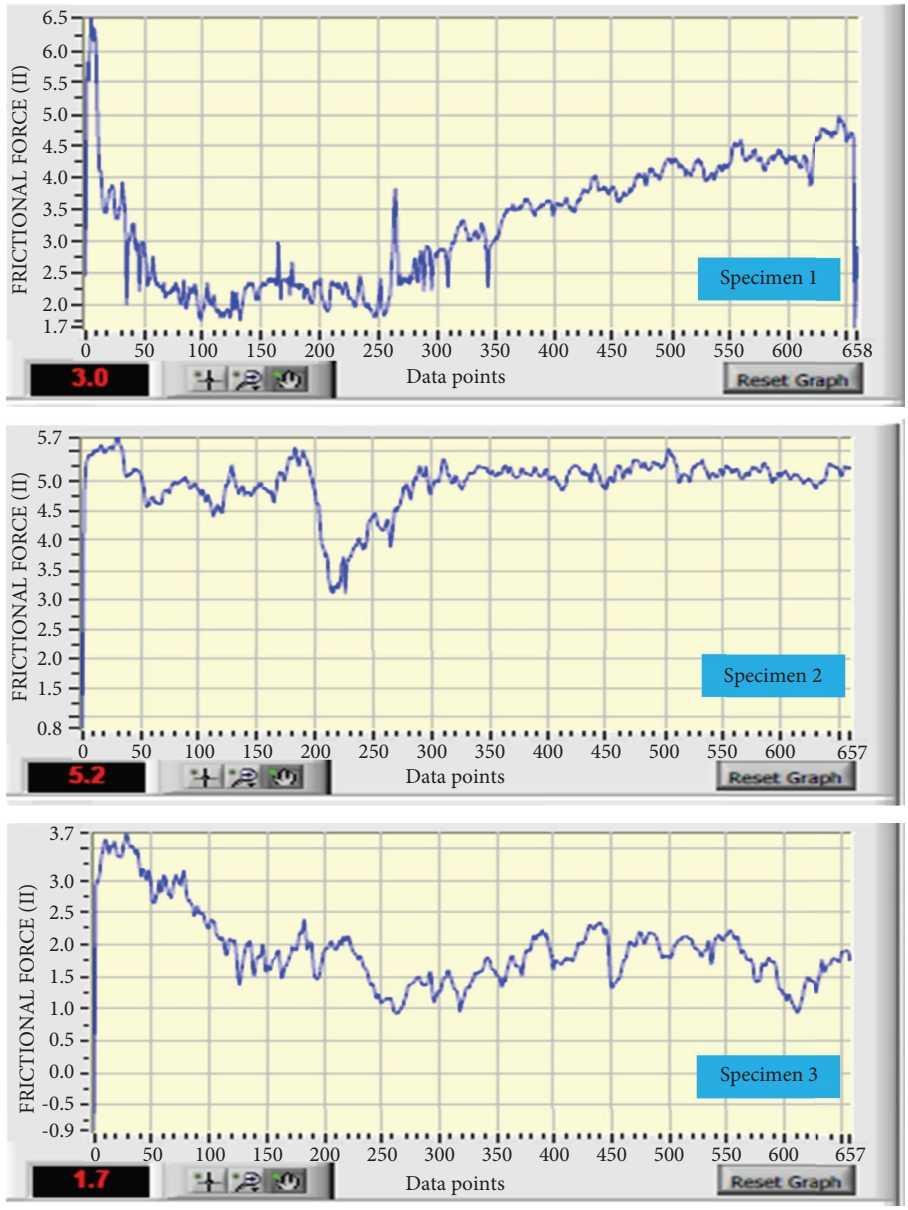

Figure 9: Frictional force vs. sliding distance curve recorded for the specimens.

distribution in the disc brake plate during the braking action. The steps such as model creation, the meshing of the model, and boundary conditions were involved in the analysis. Initially, a model of a disc brake plate was created using solid works software then the properties of the model are fed into the software using custom properties. The model creation of the disc brake plate involved extrusion, revolved cut, chamfering, etc. The model created using the standard dimensions of the disc brake plate in motorbikes is shown in Figure 11(a). The created model was in turn meshed and the mesh information was given in the figure. The maximum aspect ratio is around 4. It was done to divide the object into a fine number of elements so that the properties required can be analyzed in each element. Meshing is the primary for

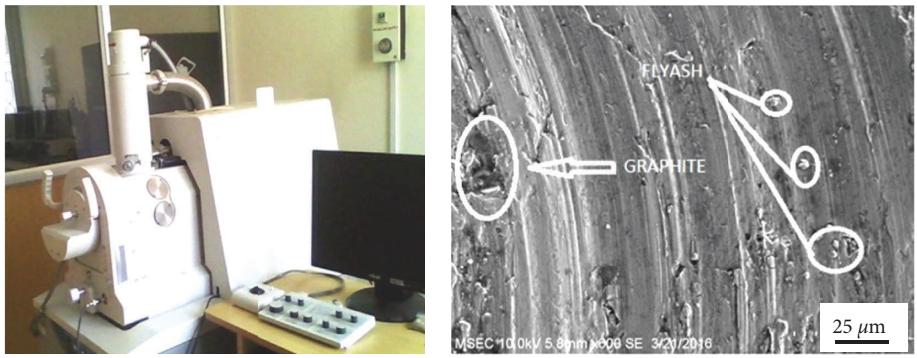

(a) (b)

Figure 10: (a) Scanning electron microscope (SEM); (b) SEM image of composite.

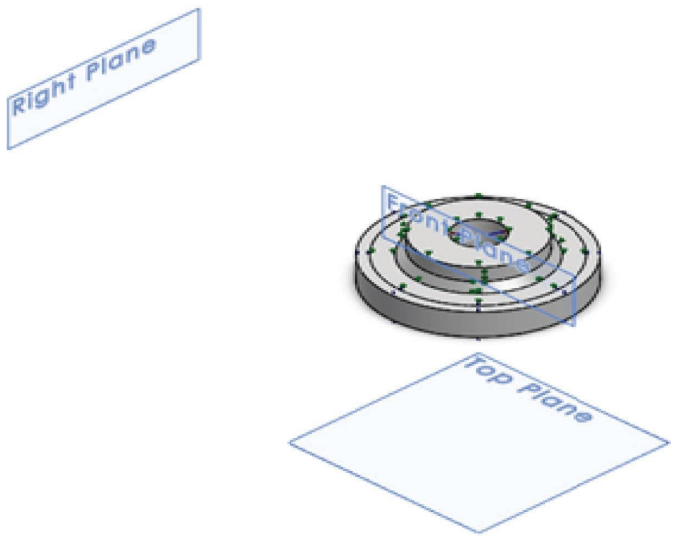

(a)

Mesh Information - Details

Total Nodes	116198
Total Elements	69940
Maximum Aspect Ratio	4.1135
% of elements with Aspect Ratio < 3	99.8
% of elements with Aspect Ratio > 10	0
% of distorted elements(Jacobian)	0
Time to complete mesh(hh;mm;ss):	00:00:07
Computer name:	KRISHNAN

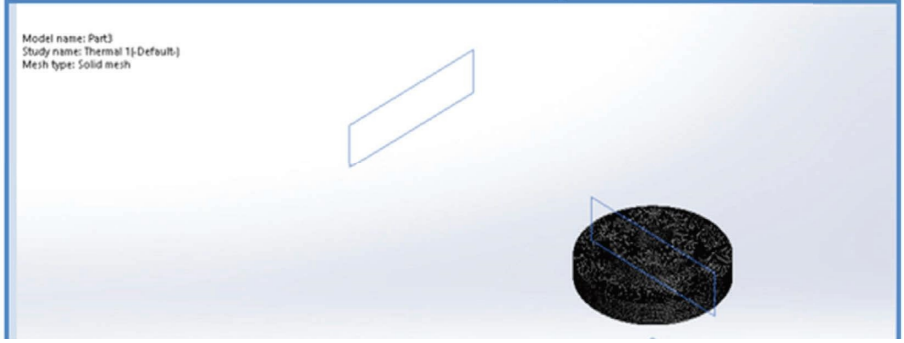

(b)

Figure 11: Continued.

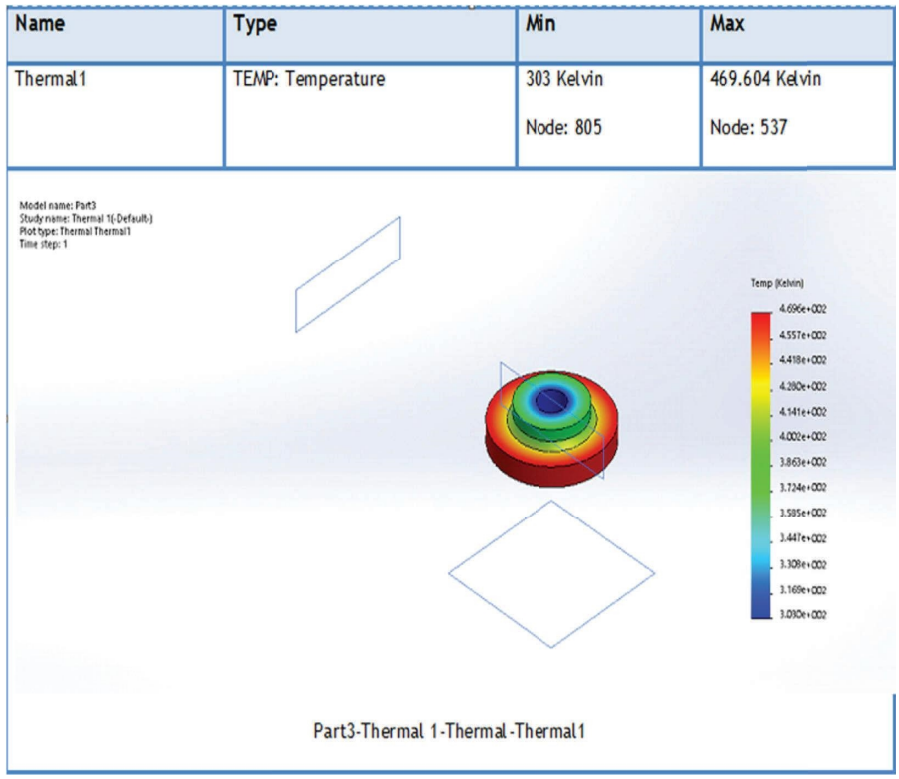

(c)

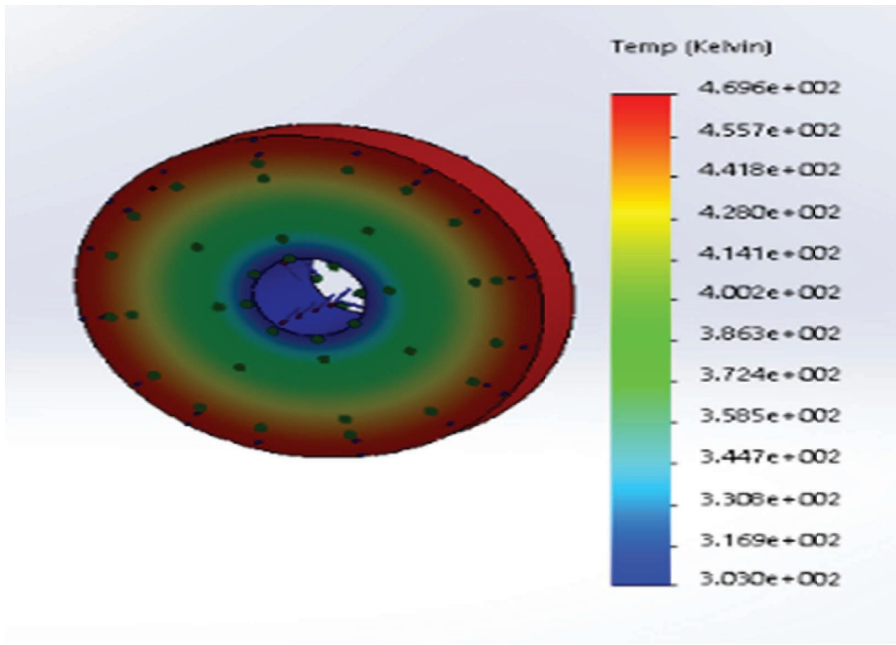

(d)

Figure 11: (a) Disc brake plate model; (b) meshing of disc brake plate model; (c) thermal analysis (top view); (d) thermal analysis (bottom view).

finite element analysis. Nevertheless, the base portion of the plate (i.e.,) hub portion was fixed as to boundary conditions while the analysis. The specified area was the area of the brake pad that was to be in contact with the plate. This particular area is sensitive and bears the pressure of braking, so a pressure of 1 MPa was applied in that area, and the results were analyzed. A maximum temperature of 469 Kelvin was recorded.

4. Conclusions

The AA2024-fly ash-graphite hybrid composite was successfully manufactured utilizing the stir casting technique, and the cast specimens were evaluated for analyzing their mechanical and tribological characteristics. The following observations are made based on the experimental findings:

(a) Addition of 10 wt. % flyash reduces the density of the composite, thereby reducing the overall weight.

(b) Excessive graphite content increases the porosity and cracks leading to a reduction in the mechanical performance of the hybrid composite.

(c) Incorporated graphite particles act as a lubricant during the abrasion process, reducing wear. The wear rate increases with applied stress, and at 5% graphite weight, the wear rate and coefficient of friction are reduced.

(d) The AA2024-flyash-graphite hybrid composite can be used in low-strength, less-weight, and high-wear applications such as low-weight gears in marine applications and low-duty motor and bike disc brakes. It could also be used for making low-strength fasteners in aerospace applications.

Data Availability

The data supporting the findings of the study are available from the corresponding author upon request.

Conflicts of Interest

The authors declare that they have no conflicts of interest.

Acknowledgments

The authors appreciate the technical assistance to complete this experimental work from the Department of Mechanical Engineering, K. Ramakrishnan college of Technology, Trichy, Tamilnadu, India. The authors would like to thank the technical assistance to complete this experimental work.

References

[1] T. Matsunaga, J. K Kim, S. Hardcastle, and P. K. Rohatgi, "Crystallinity and selected properties of flyashparticles," *Materials Science and Engineering A*, vol. 325, no. 1-2, pp. 333–343, 2002.

[2] M. K. Marichelvam, S. Senthil Murugan, K. Maheswaran, and D. ShyamprasadVarma, "Processing and Characterization of Eco-Friendly Cutting Fluid with Nano Additives for Turning Operation," *Surface Review Letters*, vol. 28, 2021.

[3] P. K. Rohatgi and B. C. Pai, "Seizure resistance of cast aluminium alloys containing dispersed graphite particles of various sizes," *Wear*, vol. 59, no. 2, pp. 323–332, 1980.

[4] P. K. Rohatgi, S. Ray, and Y. Liu, "Tribological properties of metal matrix–graphite particle composites," *International Materials Reviews*, vol. 37, no. 1, pp. 129–152, 1992.

[5] J. Zhang, R. J. Perez, and E. J. Lavernia, "Effect of SiC and graphite particulates on the damping behavior of metal matrix composites," *Acta Metallurgica et Materialia*, vol. 42, no. 2, pp. 395–409, 1994.

[6] M. K. Surappa and P. K. Rohatgi, "Technical note," *Metals Technology*, vol. 5, no. 1, pp. 358–361, 1978.

[7] B. P. Krishnan, M. K. Surappa, and P. K. Rohatgi, "The UPAL process: a direct method of preparing cast aluminium alloy-graphite particle composites," *Journal of Materials Science*, vol. 16, no. 5, pp. 1209–1216, 1981.

[8] S. Basavarajappa, G. Chandramohan, A. Mahadevan, M. Thangavelu, R. Subramanian, and P. Gopalakrishnan, "Influence of sliding speed on the dry sliding wear behaviour and the subsurface deformation on hybrid metal matrix composite," *Wear*, vol. 262, no. 7–8, pp. 1007–1012, 2007.

[9] C. B. Lin, R. J. Chang, and W. P. Weng, "A study on process and tribological behavior of Al alloy/Gr. (p) composite," *Wear*, vol. 217, no. 2, pp. 167–174, 1998.

[10] J. N. Wei, H. F. Cheng, Y. F. Zhang, F. S. Han, Z. C. Zhou, and J. P. Shui, "Effects of macroscopic graphite particulates on the damping behavior of commercially pure aluminium," *Materials Science & Engineering, A: Structural Materials: Properties, Microstructure and Processing*, vol. 325A, pp. 444–453, 2002.

[11] S. S. Murugan and T. P. D. Rajan, "Characterization of graphite-reinforced LM30-aluminium matrix composite processed through gravity and vertical centrifugal casting processes," *J. Inst. Eng. India Ser. D*, vol. 102, no. 1, pp. 19–26, 2021.

[12] S. S. Murugan, P. Sathiya, and A. N. Haq, "Mechanical properties estimation from tensile testing of aa6063-aisi304l bimetal joints friction welded with different joining methods," *Surface Review and Letters*, vol. 28, no. 04, Article ID 2150013, 2021.

[13] P. Zhang, S. X. Li, and Z. F. Zhang, "General relationship between strength and hardness," *Materials Science and Engineering A*, vol. 529, pp. 62–73, 2011.

[14] D. Norris, J. Reaugh, and W. Server, "A fracture-toughness correlation based on Charpy initiation energy," in *Fracture Mechanics*, R. Roberts, Ed., pp. 207–217, ASTM International, West Conshohocken, PA, USA, 1981.

[15] G. T. Méndez, S. I. C. Colindres, J. C. Velazquez, D. A. Herrera, E. T. Santillan, and A. Q Bracarense, "Fracture toughness and Charpy CVN data for A36 steel with wet welding," *Soldagem&Inspeção*, vol. 22, no. 3, pp. 258–268, 2017.

[16] J. R. Dougan, *Relationships between Charpy V-Notch Impact Energy and Fracture Toughness*, Web, [PWR; BWR], USA, 1982.

[17] J. Kapp and J. H. Underwood, "Correlation between Fracture Toughness, Charpy V-Notch Impact Energy, and Yield Strength for ASTM A723 Steel," *Me-Morandum Report ARCCB-MR-92008*, 1992.

[18] M. V. Krishna and A. M. Xavior, "An investigation on the mechanical properties of hybrid metal matrix composites," *Procedia Engineering*, vol. 97, pp. 918–924, 2014.

[19] A. Saravanakumar, P. Sasikumar, and S. Sivasankaran, "Synthesis and mechanical behavior of AA 6063-X wt% Al2O3- 1% Gr (X = 3, 6, 9 and 12 wt%) hybrid composites," *Procedia Engineering*, vol. 97, pp. 951–960, 2014.

[20] J. O. Bird, P. J. Chivers, 28 - Friction, J. O. Bird, and P. J. Chivers, *Newnes Engineering and Physical Science Pocket Book*, Elsevier, Amsterdam, Netherlands, 1993.

[21] R. N. Rao and S. Das, "Effect of sliding distance on the wear and friction behavior of as cast and heat-treated Al–SiCp composites," *Materials & Design*, vol. 32, no. 5, pp. 3051–3058, 2011.